Competing CO···CO, C–H···O, Cl···O, and Cl···Cl Interactions Governing the Structural Phase Transition of 2,6-Dichloro-p-benzoquinone at Tc = 122.6 K

ARTICLE *in* CRYSTAL GROWTH & DESIGN · AUGUST 2013

Impact Factor: 4.89 · DOI: 10.1021/cg401123s

7 AUTHORS, INCLUDING:

Riccardo Destro
University of Milan
127 PUBLICATIONS **1,762** CITATIONS
SEE PROFILE

Laura Loconte
University of Milan
16 PUBLICATIONS **46** CITATIONS
SEE PROFILE

Raffaella Soave
Italian National Research Council
51 PUBLICATIONS **438** CITATIONS
SEE PROFILE

Leonardo Lo Presti
University of Milan
63 PUBLICATIONS **346** CITATIONS
SEE PROFILE

CRYSTAL GROWTH & DESIGN

Article

pubs.acs.org/crystal

Competing C═O···C═O, C−H···O, Cl···O, and Cl···Cl Interactions Governing the Structural Phase Transition of 2,6-Dichloro-*p*-benzoquinone at T_c = 122.6 K

Riccardo Destro,*[,†,‡] Elisabetta Sartirana,[†] Laura Loconte,[†] Raffaella Soave,[‡] Pietro Colombo,[‡] Claudio Destro,[§] and Leonardo Lo Presti[†,‡,∥]

[†]Department of Chemistry, Università degli Studi di Milano, Via Golgi 19, I-20133 Milano, Italy

[‡]Istituto di Scienze e Tecnologie Molecolari (ISTM), CNR, Via Golgi 19, I-20133 Milano, Italy

[§]MECLAM, Largo Cantieri Monti 5, I-20863 Concorezzo, Italy

[∥]Centre for Materials Crystallography, Aarhus University, Langelandsgade 140, DK-8000, Aarhus, Denmark

Supporting Information

ABSTRACT: 2,6-Dichloro-*p*-benzoquinone (DCBQ) has been investigated by single-crystal X-ray diffraction experiments in the *T* range of 300−21 K and quantum-mechanical simulations. A reversible monoclinic (high-T) to triclinic (low-T) phase transition has been detected at T_c = 122.6(5) K. The various noncovalent interactions (NCIs) that determine the solid-state self-recognition of DCBQ have been characterized as a function of *T* through the quantum theory of atoms in molecules. On lowering *T*, carbonyl−carbonyl interactions progressively strengthen, inducing a change in the crystal structure, while the dipolar C−Cl···O═C NCIs and the relatively strong Cl···Cl halogen bonds (XBs) and CH···O hydrogen bonds play an essential, but ancillary, role. Dispersive forces cooperate with other closed-shell dipolar NCIs, and particularly with XBs, in determining their overall attractive character, even when bulky and positively charged chlorine atoms are drawn closer and closer at low temperatures. The intermolecular interaction energies have been evaluated above and below T_c as sums of electrostatic, repulsion, and dispersion contributions.

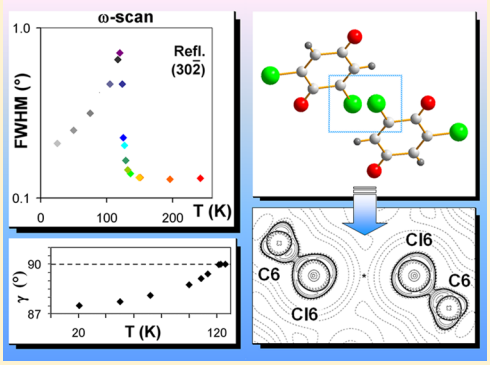

1. INTRODUCTION

Halogen bonding (XB) is a crucial factor in governing the molecular recognition of halides, the structural control of molecular materials (including biomacromolecules), and the crystal packing of halogenated hydrocarbons.[1] It is a ubiquitous electrostatic noncovalent interaction (NCI) that occurs between the charge depletion zone ("*σ*-hole") in the valence shell of a halogen X atom at the edge of an R−X bond (R usually being a carbon atom and X mainly Cl, Br, and I), and a region of charge concentration (e.g., lone pairs, *π* density) of a nearby electron-rich system Y. The anisotropy of the charge density distributions around the X and Y species usually determines the high directionality observed in XBs.[2] Therefore, by tuning the structure and geometry of specific reactant synthons bearing suitable X and Y substituents, it is possible, for example, to effectively synthesize coordination (co)-polymers exhibiting the desired network topology.[1,3]

To gain insight into the driving forces underlying the self-assembly process, the accurate knowledge of the interaction energies of halogen-bonded molecular pairs is mandatory, especially when other functional groups, able to significantly contribute to the overall crystal cohesive energy, are present.[3] Actually, the molecular (self-)recognition mechanism relies on how the *overall* charge density distributions of the individual synthons interact with each other,[4] or, equivalently, on the mutual interplay among *all* the relevant chemical groups present in the molecule. Indeed, even when strong XBs are set up in the crystal, other interactions may as well play a crucial role in governing the observed crystal structure and packing. The study of the mutual interplay among XBs and competing NCIs[3,5] can, therefore, pave the way to the developing of more efficient synthetic strategies.

In this context, we focus here on a very interesting test case of C−Cl···Cl XBs competing with dipolar C═O···C═O, C−Cl···O═C, and CH···O NCI's, namely, the phase transition of the solid-state quinone derivative 2,6-dichloro-*p*-benzoquinone (DCBQ, Scheme 1). More in detail, we aim at (i) disclosing the relevant features of the DCBQ crystal structure in the high- and low-T phases, from both the crystallographic and charge density viewpoints; (ii) analyzing the various contributions to the total intermolecular interaction energy in both the phases;

Received: July 25, 2013
Revised: August 30, 2013
Published: August 30, 2013

Scheme 1

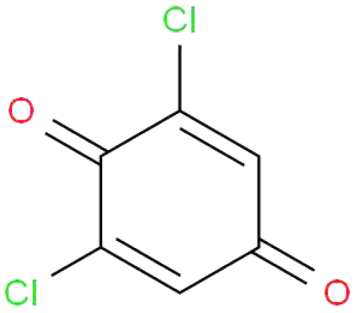

and (iii) determining the role played in the phase transition by the most crucial directional intermolecular NCIs.

DCBQ is an electron acceptor widely employed in studies of the photosystem II[6,7] and in investigations of electron-transfer processes.[8−10] It has been also reported as an efficient reagent to form cycloadducts[11,12] and optically active hydroquinones.[13] More recently, a paper[14] on the ground-state electronic structure of charge-transfer complexes reported for DCBQ (one of the 30 investigated acceptors) the values of electron affinity (EA) computed with several DFT methods: in agreement with the experimental findings (referred to in the same paper), the computed EA of the dichloro-substituted quinone is much closer to that of the 2,3,5,6-tetrachloro-*p*-benzoquinone (chloranil) than to the EA of the unsubstituted 1,4-benzoquinone.

The X-ray diffraction (XRD) room-temperature (RT) crystal structure of DCBQ was determined long ago[15] from diffractometer measurements. Previous Weissenberg films had shown[15] rapidly decreasing intensities as the Bragg angles increased, with no signal above background for $((\sin\theta)/\lambda) > 0.55$, but no disorder was observed. Rather, the crystal packing included three intermolecular distances significantly shorter than the sum of the van der Waals radii of the atoms involved: a Cl···Cl separation of 3.33 Å, an O···H distance of 2.46 Å, and, most remarkably, an O···C contact as short as 2.84 Å.

To gain a detailed understanding of the nature and mutual interplay of such intermolecular interactions, we planned an experimental determination of the electron density distribution in crystalline DCBQ, to be obtained by multipole analysis of its low-temperature (LT) XRD structure factors. However, while slowly cooling the single-crystal sample, mounted on a diffractometer, at steps of 10−20 K, profile anomalies (peak enlargement and/or doubling) for most of the reflections were detected at $T < 130$ K. Later visual inspection of the sample excluded any crystal rupture. Furthermore, when the sample was brought back to $T = 130$ K, all anomalies disappeared, while returning down to $T < 120$ K, the abnormal profile shapes were observed again. Such a behavior was always reproduced by cycling several times through the same temperature range. All of this led to the conclusion that a reversible phase transition, associated with crystal twinning, was occurring at a temperature between 120 and 130 K. Indeed, our subsequent work confirmed that DCBQ undergoes a displacive, second-order monoclinic (high-T) to triclinic (low-T) phase transition at $T \approx 122-123$ K.

The paper is organized as follows: First, the methods adopted to estimate the transition temperature (T_c) from single-crystal XRD data are described. Then, the crystal packing features and self-recognition energetics are analyzed on the basis of the charge density analysis of solid DCBQ in the two phases, as performed from both experimental and theoretical (DFT) structure factors (F's) at 135 K and only theoretical F's at 21 K. Then, the importance of various kinds of NCIs in determining the observed structure changes between RT and 21 K is discussed.

2. EXPERIMENTAL SECTION

2.1. Single-Crystal X-ray Data Collections. All XRD measurements were done on the same specimen, whose quality remained good for months and started to become modest only after ≈30 passages through the transition temperature. The sample employed for this study was obtained by recrystallization of commercial (Sigma Aldrich) DCBQ from *n*-hexane by slow evaporation of a solution in a refrigerator ($T \approx 4$ °C). To avoid sublimation effects,[16] the specimen was sealed in a Lindemann glass capillary and mounted on a four-circle Siemens P4 diffractometer, equipped with the local version of a Samson cryostat[17] we had used for most of our previous[18,19] X-ray single-crystal charge density studies between 20 and 100 K. Substantial modifications (designed and manufactured by two of us, R.D. and C.D.) were required to adapt the cryostat, originally mounted on a Syntex $P\bar{1}$ diffractometer, to the P4 instrument; yet the final performances were of the same previous high quality and reproducibility. Reflection intensities and profiles, all measured with Mo Kα radiation ($\lambda = 0.71073$ Å), were recorded by a carefully adjusted and optimized point detector. Full details of our instrumental settings for temperature control and accuracy in a phase transition study can be found elsewhere.[20]

Three series of multi-T measurements were performed to estimate the transition temperature T_c: (i) the full width at half-maximum (FWHM) of six strong reflections; (ii) the intensities of the equatorial *h*0*l* reflections; and (iii) the crystal unit cell dimensions. Furthermore, to determine the high-T crystal structure, intensity measurements of charge-density quality were performed at $T = 135$ K, after a conventional RT collection for comparison with the literature report.[15] Limited sets of data were instead collected at $T = 21$ K, owing to extensive partial overlap of the diffraction pattern from the two components of the twin.

2.2. Determination of the Phase-Transition Temperature. *2.2.1. FWHM of Reflection Profiles.* Three strong reflections and their Friedel mates were accurately centered at 16 different temperatures in the range of 25−242 K. Scans in the ω and $\theta-2\theta$ mode at a rate of 2°/min were recorded for each reflection just after its centering. The corresponding 96-step profiles were plotted, and their FWHM were evaluated. Two of the reflections, with indexes −2 1 3 and −2 −1 3, showed peak splitting (with increasing peak separation as T was decreasing) at $T < 123$ K in their ω-scan plots, but not in the $\theta-2\theta$ plots. By contrast, no splitting was observed for the third reflection, the equatorial 3 0 −2, the profile of which presented a marked broadening on lowering the temperature from 132 to 120 K, followed by a reduction of the peak width in the temperature range of 120−25 K. The overall behavior of this ω-scan profile is reported in Figure 1, with individual values listed in Table S1 (Supporting Information). Repeated recordings of the plot, by randomly increasing or decreasing the temperature in the full 25−242 K range, reproduced the profile shape, at a given temperature, within experimental uncertainty.

2.2.2. Intensity Measurements of Low-T Phase h0l Reflections. From the intensity data collected at $T = 21$ K (see below), the 14 strongest reflections of indexes *h*0*l* with $l = 2n + 1$, which are systematically extinct in the high-T monoclinic phase, were selected and centered at 26, 50, and 73 K, with recording of the integrated intensity at the end of each centering process. The only monoclinic 0*k*0 systematic extinction that had shown $I > 0$ at 21 K, which is the reflection 0 −3 0, was also included among the investigated reflections, but at $T = 90$ K it was too weak to be reliably centered. Since the same occurred to some other components of the set, intensity measurements of the 15 reflections at $T > 90$ K were performed as part of standard data collections of all *h*0*l* reflections within $((\sin\theta)/\lambda) = 0.6$ Å^{-1}. Each collection was preceded by a regular determination of the orientation matrix at the corresponding temperature. Intensities were

dx.doi.org/10.1021/cg401123s | *Cryst. Growth Des.* 2013, 13, 4571−4582

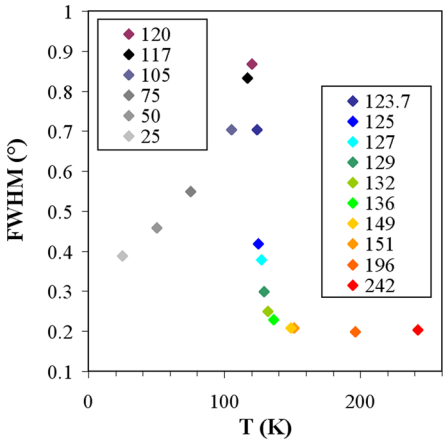

Figure 1. Full width at half-maximum (FWHM) for the ω-scan profile of reflection 3 0 −2 as a function of the temperature. Uncertainties are <1 K for T and approximately half the diamond size for the widths.

so acquired at 90, 100, 110, 120 (twice), and 122 K. At the latter temperature, only the two strongest of the 14 $h0l$ reflections of the original 21 K set, that is, reflection 5 0 −3 and its Friedel mate, had $I > 3\sigma(I)$.

2.2.3. Multitemperature Measurement of Cell Parameters. Cell dimensions were determined at 18 different temperatures between 20 and 300 K. At each temperature, the setting angles of one or two sets of reflections were optimized in both the positive and the negative 2θ regions, to cancel possible instrumental biases. Only one set was employed for the measurement of the monoclinic cell, while at $T <$ 120 K, one set per each of the two components of the twin was centered (except for T = 108.6 K, where only one component was investigated). As in the case of our study of the phase transition of 3,4-bis(dimethylamino)-3-cyclobutene-1,2-dione (DMACB) at 147 K,[20] the cell parameters were obtained by a least-squares fit to the resulting values of $\sin^2\theta$ and are reported in Table S2 (Supporting Information).

2.3. Data Treatment and Structure Refinement at T = 300, 135, and 21 K. Full details of X-ray data collection and refinement for DCBQ at the three temperatures are given in Table 1. All intensities were analytically corrected for absorption,[22] and their refinement was based on F^2. For the RT and 21 K data, the program SHELXL97[23] was employed, following the conventional, spherical atom procedure, while multipole refinements were carried out with the VALRAY system of programs[21] on the T = 135 K data set. The multipole model, based on the Stewart formalism,[24] included hexadecapole terms for the two Cl atoms, octupoles for C and O atoms, and quadrupoles for the H atoms, for which anisotropic displacement parameters (ADP's) were also evaluated.[25] The set of electron population parameters at convergence was then employed to map in real space, via multipole functions, the experimental electron density $\rho_{EXP}(\mathbf{r})$.

Diffraction intensities of the low-T phase were obtained from both components of the twin and then merged, after careful examination to reject those showing irregular profiles due to overlap, that affected ≈31% of the data. Scaling of the two sets gave an average intensity ratio of 1.17 and the equatorial $h0l$ intensities, all showing nonsplit profiles and shared by both elements of the crystal, were accordingly adjusted.

Final atomic coordinates and thermal parameters at the three temperatures are deposited as CIF files (Supporting Information); the corresponding bond distances and angles are reported also in Table S3 (Supporting Information).

Table 1. Crystallographic and Refinement Details for DCBQ

sample information			
empirical formula	$C_6H_2O_2Cl_2$		
crystal size/mm^3	0.70 × 0.35 × 0.08		
formula wt/g mol^{-1}	176.986		
F(000)	352.0		
T/K	300	135	21
crystal system	monoclinic	monoclinic	triclinic
space group	$P2_1/c$	$P2_1/c$	$P\bar{1}$
Z	4	4	4
a/Å	9.066(2)	8.940(1)	8.906(3)
b/Å	5.500(2)	5.426(1)	5.370(2)
c/Å	17.754(4)	17.359(2)	17.214(6)
α/deg	90.0	90.0	90.40(3)
β/deg	126.54(3)	125.08(1)	124.31(3)
γ/deg	90.0	90.0	87.53(4)
V/Å^3	711.3(4)	689.1(2)	679.2(5)
D_x/g cm^{-3}	1.653	1.706	1.731
μ/mm^{-1}	0.84	0.87	0.88
data collection			
$((\sin\theta)/\lambda)_{max}$/Å^{-1}	0.600	1.003	0.600
no. collected reflns	1741	21034	7766
no. unique reflns	1257	5821	2211
R_{merge}	0.013	0.046	0.085
no. of reflns with $[F^2 > 2\sigma(F^2)]$	833	2113	1847
refinement results[a]			
GOF	1.053	1.084	1.009
$R(F)$	0.0432	0.0307	0.0456
wR(F^2)	0.0965	0.0540	0.1255
no. variables	100	289	193

[a]For data at 300 and 21 K, the refinement was based on all unique reflections. At T = 135 K, only the data with $[F^2 > 2\sigma(F^2)]$ were used in the least-squares refinement by VALRAY.[21]

dx.doi.org/10.1021/cg401123s | Cryst. Growth Des. 2013, 13, 4571−4582

3. THEORETICAL METHODS

The theoretical charge density model $\rho_{THEO}(\mathbf{r})$ of crystalline DCBQ has been derived from theoretical structure factors for both the high-T and the low-T crystal structures. Crystal cohesive energies have been also evaluated for both the solid phases.

3.1. Theoretical Structure Factors. Fully periodic single-point DFT calculations at both the 135 and the 21 K experimental geometries were carried out with the CRYSTAL2006 program,[26] adopting the B3LYP[27] hybrid-type functional and the Pople's standard molecular 6-31G** basis set.

Static structure factors for all independent reciprocal-lattice points (5821 in number at T = 135 K and 11 484 at 21 K) included within $((\sin\theta)/\lambda)$ = 1.003 (the same limit of the 135 K X-ray experiment) were obtained through the Fourier transform of the periodic density and employed in the code VALRAY[21] to derive a multipole-projected charge density for both phases.

At convergence, the least-squares refinement of 276 multipole population parameters (up to hexadecapoles for Cl, O, and C atoms, quadrupoles for H atoms, plus two radial parameters, α and κ in VALRAY,[21] for each of the three atomic species Cl, O, and C) gave $R(F)$ = 0.0050 and $wR(F^2)$ = 0.0098 for the set of 135 K data. Corresponding quantities for the low-T set were 538 multipole parameters plus the same 6 radial parameters, $R(F)$ = 0.0050 and $wR(F^2)$ = 0.0099.

The topological analysis of the ρ_{THEO} (at T = 21 and 135 K) and ρ_{EXP} (at T = 135 K) distributions was performed in the mainframe of Bader's QTAIM (quantum theory of atoms in molecules),[28] by the program PAMoC.[29] For comparison purposes, we have also analyzed with the same program the topology of the charge density of isolated DCBQ, as obtained by the Gaussian 09 software[30] after geometry optimization at both the B3LYP/6-31G** and the B3LYP/6-311+G* theory levels.

3.2. Crystal Energies. Crystal cohesion energies were obtained as sums of pairwise molecular interaction energies between a reference molecule and the remaining molecules in the crystal. The experimental charge-density approach (ECDA) to intermolecular interactions pioneered by Spackman[31] was followed, where the electrostatic energy, E_{es}, is derived from atom-centered electrostatic moments as derived from the ρ distribution and is combined with empirical exchange-repulsion, E_{rep}, and dispersion, E_{disp}, energies:

$$E_{interaction}\ (\mathrm{ECDA}) = E_{es} + E_{rep} + E_{disp}$$

The values of E_{es} have been obtained from the QTAIM partitioning of the ρ_{THEO} distributions through the Buckingham-type (moment−moment, MM) scheme,[32] corrected for the promolecule energy, according to the strategy recently proposed[31a] and implemented in the code PAMoC.[29] In this approach, the E_{es} is expressed as a sum of promolecule−promolecule, promolecule−deformation, and deformation−deformation terms:

$$E_{es} = E_{pro-pro} + E_{pro-def} + E_{def-def}$$

The classical E_{disp} and E_{rep} terms have been modified with respect to the original Spackman's formulation, in that the atomic parameters included in the E_{rep} potential have been optimized to fit ab initio repulsion energies,[29] whereas the atomic parameters C_6 included in the dispersion term have been refined against a set of 87 intermolecular C_6 coefficients: 77 from experimental dipole oscillator strength distributions (DOSDs) and 10 from ab initio theory calculations of nucleic acid base pairs.[29]

All the calculations were done for 600 interacting molecular pairs in each of the two crystal phases. Outside this cluster, additional molecules were considered, for a total of about 2200 unit cells around the reference one, with the corresponding electrostatic energy contributions being computed using overall molecular moments.

4. RESULTS AND DISCUSSION

4.1. Nature of the Transition and Value of T_c. The strong temperature dependence shown by the intensities of the low-θ equatorial reflections $h0l$ with $l = 2n + 1$ (see the Experimental Section above), together with the behavior of the cell angles α and γ in the temperature range of 25−130 K (see Table S2 in the Supporting Information and Figure 2), indicates that DCBQ undergoes a continuous (displacive) second-order phase transition with T_c in the range of 120−125 K.

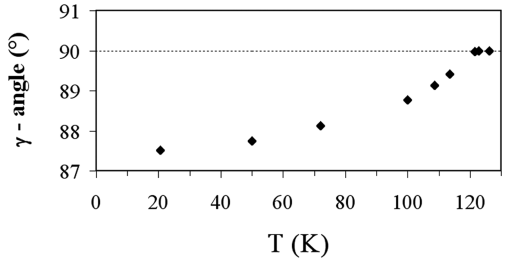

Figure 2. Unit cell angle γ of DCBQ in the temperature range of 20.5−130 K.

A first estimate of the transition temperature can be obtained from the quantities reported in the lambda-shaped graph of Figure 1: the straight line through the two points at T = 125.0 and 123.7 K intersects, at T = 122.8 K, the second-order polynomial through the points at the three subsequent lower temperatures. To a first approximation, this intersection T can be assumed as T_c.

A very similar value is obtained by fitting the experimental measurements of the γ angle (Figure 2) to a quadratic expression and then intersecting the resulting line with the horizontal straight line at γ = 90°. The best fit and the smallest estimated standard deviation (esd) is given by a least-squares treatment (with x = angle value and y = temperature) that includes six individual measurements, two at $T \approx$ 121.5 K and four at T = 113.5−114.0 K. The resulting T_c is 122.6 ± 0.5 K.

A third procedure to evaluate T_c is reported in Figure 3: the intensities of the two strongest $h0l$ reflections with $l = 2n + 1$ in the T range of 90.6−122.5 K (reflection 5 0 −3 and its Friedel mate) are fitted to a straight line that gives null intensity at T_c = 122.5 ± 0.2 K. We may safely conclude that the structural phase transition of DCBQ occurs at T_c = 122.6 ± 0.5 K.

4.2. The High-T Monoclinic Phase of DCBQ vs That of Chloranil. At both RT and T = 135 K, the carbonyl closer to the two chlorine atoms, that is, C1═O1 in Figure 4a, has a bond length shorter than that of C4═O4 by 0.014 Å, which is about 7 times the esd at the lower T. This difference is consistent with that (0.012−0.013 Å) shown by the gas-phase-optimized geometries. The two C−Cl bonds, after correction

dx.doi.org/10.1021/cg401123s | Cryst. Growth Des. 2013, 13, 4571−4582

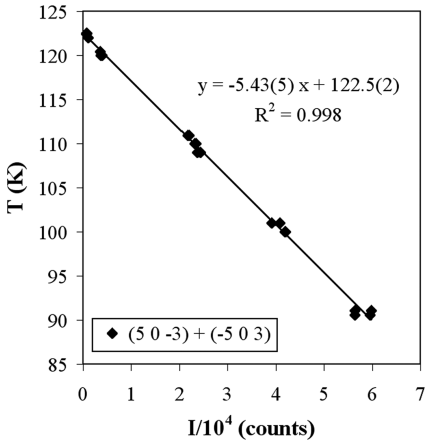

Figure 3. Temperature dependence of X-ray diffracted intensities $I_{5\,0\,-3}$ and $I_{-5\,0\,3}$.

for thermal motion,[33] have the same length within experimental uncertainty, 1.724(1) Å, at both temperatures. The calculated gas-phase value is 1.732−1.733 Å. The polarized H atom model[34] we adopted for the VALRAY multipole refinement gives values of 1.05(1) and 1.09(1) Å for the C3−H3 and C5−H5 bond lengths, respectively, to be compared with 0.88(2) and 0.99(2) Å out of the spherical atom refinement with SHELX at 135 K.

The most relevant structural feature of crystalline DCBQ in its high-T phase is the zigzag (or helix) arrangement of molecules related by a 2_1 screw axis (Figure 4), with an intermolecular C═O···C═O separation of 2.842(5) Å at RT that shortens to 2.765(2) Å at T = 135 K (the reduction practically matches the shrinkage of the b axis, 0.074 Å). The resulting herringbone type of molecular packing is very similar to that of chloranil,[35] as described and discussed by Rees,[15] who noted, in particular, that not only the O···C distance is the same within experimental error, but also the O···C═O angles coincide, within 1°, in both RT crystals. The comparison with chloranil is of special interest, since this compound also

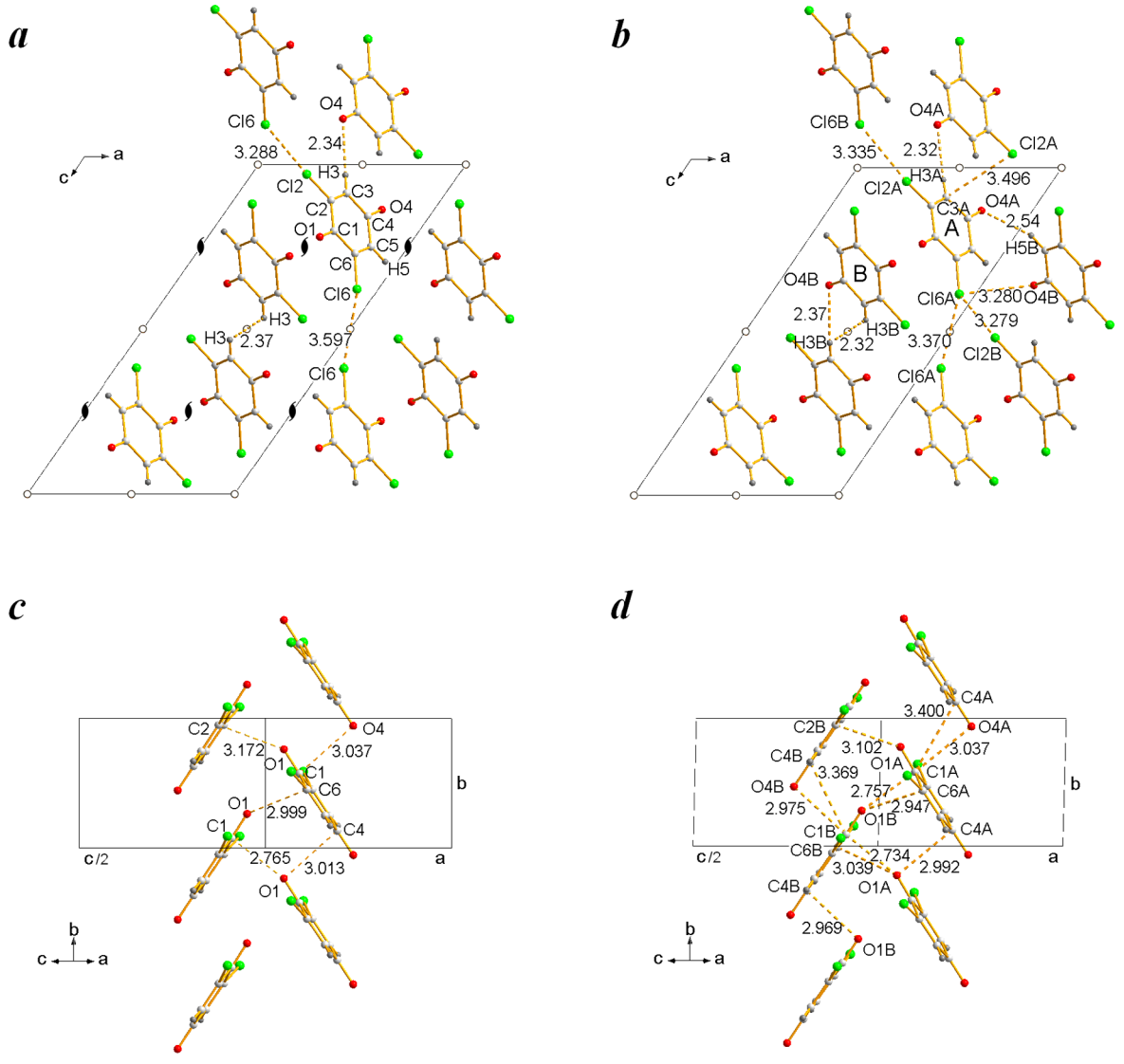

Figure 4. Crystal packing of DCBQ with intermolecular contacts shorter than the sum of van der Waals radii. View down the b axis (a, b) and the 2, 0, 1 direction (c, d). High-T phase at 135 K: (a) and (c). Low-T phase at 21 K: (b) and (d). For the sake of comparison, the contacts at 21 K involving H atoms come from modified C−H bond lengths (see text).

dx.doi.org/10.1021/cg401123s | *Cryst. Growth Des.* 2013, 13, 4571−4582

Table 2. QTAIM Atomic Charges q (Electrons) and Volumes V (Å^3) (First Line: High-T Phase. Second and Third Lines: Low-T Phase, Molecules A and B, Respectively)

atom	charge[a]/e	volume[b]/Å^3	atom	charge[a]/e	volume[b]/Å^3
C1	0.913(6)	7.75	O1	−1.051(6)	16.33
C1A	0.906(6)	6.77	O1A	−1.091(7)	16.40
C1B	0.918(6)	7.65	O1B	−1.123(7)	16.80
C2	−0.037(6)	10.42	Cl2	0.055(8)	27.36
C2A	−0.027(7)	10.04	Cl2A	0.077(9)	27.96
C2B	−0.027(7)	10.30	Cl2B	0.067(8)	28.17
C3	−0.010(6)	11.20	H3	0.135(4)	5.73
C3A	0.003(7)	11.14	H3A	0.141(5)	5.62
C3B	0.008(7)	10.98	H3B	0.137(5)	5.66
C4	0.855(6)	7.79	O4	−1.015(6)	16.16
C4A	0.842(6)	7.85	O4A	−1.040(7)	16.17
C4B	0.817(6)	7.90	O4B	−1.019(7)	16.17
C5	−0.014(6)	11.29	H5	0.144(4)	5.96
C5A	0.003(7)	11.25	H5A	0.148(5)	5.85
C5B	−0.011(7)	11.22	H5B	0.161(5)	5.79
C6	−0.031(6)	10.37	Cl6	0.058(8)	27.22
C6A	−0.012(7)	9.73	Cl6A	0.073(9)	28.00
C6B	−0.031(7)	10.36	Cl6B	0.080(9)	28.19
			molecule	0.002(21)	157.57
			mol A	0.023(24)	156.79
			mol B	−0.023(24)	159.19

[a]esd's in parentheses refer to the last significant digit. [b]esd's < 0.01 Å^3.

undergoes a displacive phase transition, widely investigated by a variety of techniques,[36,37] with $T_c \approx 91-94$ K.

The other short distances of DCBQ involving ring C atoms and carbonyl O atoms are 3.06−3.24 Å long at RT and 0.06−0.08 Å shorter at 135 K (Figure 4c). Similar RT values were found in chloranil, where about the same shortening occurs on lowering the temperature to 128[16] or 110 K.[38] As for the remaining intermolecular contacts, the closest halogen−halogen separation is 3.58 Å long in RT chloranil, whereas, in DCBQ at 300 K, we observe (Table S4, Supporting Information) a Cl···Cl contact of 3.325(1) Å, which shortens to 3.288(1) Å at 135 K (Figure 4a), well below the sum of van der Waals radii (svdWr, with radius values of 1.8, 1.7, 1.5, and 1.2 Å for Cl, C, O, and H, respectively). Furthermore, the packing of DCBQ includes a short O···H separation between atoms of two neighboring helices, the RT distance being 2.64(3) Å in our structure determination and 2.46 Å in that of Rees[15] (who did not refine the positional parameters of the H atoms). The length of this H-bond amounts to 2.51(2) Å at 135 K in our spherical atom model and to 2.34(1) Å in the VALRAY multipole refinement with polarized H atoms.[34]

We might conclude that, in its monoclinic phase, the crystal packing of DCBQ is tighter (hence, it is expected to bear a more negative lattice enthalpy) than that of the high-T phase of chloranil. Yet, the melting point of the former compound is 121−124 °C, whereas that of the second is 290 °C. This is likely the consequence of the more symmetric shape of chloranyl (D_{2h}) with respect to DCBQ (C_{2v}), which implies a lower melting entropy (and, therefore, an overall higher melting temperature[4]) of the fully chlorinated compound. Furthermore, the RT thermal motion analysis of the two crystals reveals that the rms amplitudes of translational and librational motion of DCBQ, reported in Table S5 (Supporting Information), are systematically larger than those of chloranil[35] by 21−33% and 17−53% for translational and librational displacements, respectively. This suggests that the vibrational contribution to the solid-state entropy of the monoclinic high-T phase of DCBQ should be higher than that of chloranil, revealing that the relative phase stability of these chlorinated quinones depends on the close interplay of several thermodynamic factors, still far from being fully understood and possibly worthy of further studies.

4.3. The Low-T vs the High-T Phase. On lowering the temperature of the DCBQ crystals from 135 to 21 K, the molecules undergo rotations and translations that cause a change of space group from $P2_1/c$ to $P\bar{1}$. The quantities of Figure 1 and Table S1 (Supporting Information) indicate that significant displacements start at about 130 K, where a first noticeable increase of the FWHM values is observed on going to T_c from above. The breaking of the monoclinic symmetry occurs at ≈123 K, with the initial appearance of reflections that were forbidden at higher temperatures. The process of molecular displacements is continuous on decreasing the temperature, partly reminiscent of that of chloranil, for which an experimental determination of the molecular rotations at four temperatures below T_c was carried out by neutron diffraction.[37] In that case, the change was from space group $P2_1/a$ to $P2_1/n$, with a doubling of the unit cell along the c axis and a loss of one set of 2_1 screw axes, namely, those connecting molecules within the helices. For DCBQ, the total loss of the glide symmetry implies that the asymmetric unit be formed, below T_c, by two independent molecules, labeled A and B in Figure 4, that were symmetry-related (by the screw axis) above T_c. Consequently, the number of unique intermolecular contacts doubles on going from the high-T to the low-T phase, but for most of the shortest separations of the monoclinic structure, the difference between the two corresponding distances of each pair at 21 K does not exceed 0.1 Å.

Three features of the crystal packing at 21 K are of special note: (i) The two closest independent molecules A and B have their four atoms of the two carbonyl groups separated, on

dx.doi.org/10.1021/cg401123s | Cryst. Growth Des. 2013, 13, 4571−4582

average, by ≈0.10 Å less than half the periodicity along b that was required by the monoclinic symmetry. Correspondingly, the shortest O···C═O separation at 135 K, 2.765(2) Å, becomes even shorter, 2.757(4) and 2.734(4) Å. Hence, the carbonyl−carbonyl attractive interactions are stronger at T = 21 K than at T = 135 K. (ii) The CH···O hydrogen bond lengthens from 2.34(1) to 2.37(3) Å in the case of H3B···O4B, but shortens to 2.32(3) Å for H3A···O4A. On average, and in view of the high esd's, the strength of this interaction remains the same in both phases. (iii) The Cl6···Cl6 contact through a center of inversion, 3.597(1) Å long at 135 K, lengthens to 4.179(1) Å for the separation Cl6B···Cl6B, but shortens to 3.370(1) for Cl6A···Cl6A. This is the most remarkable exception to the generally modest difference within each pair of corresponding distances, as described above.

The same atom Cl6A remains very close (actually even slightly closer) to atom Cl2B of a neighboring molecule, at 3.279(1) Å vs 3.288(1) Å at T = 135 K, and becomes 0.172 Å closer to atom O4B of a third contiguous molecule (the B molecule at 1 + x, 1 + y, z). The reduction of this last separation from 3.452(1) Å at 135 K to 3.280(3) Å is paralleled by that between atom O4A and atom H5B at 1 + x, y, z, with distances of 2.71(2) Å at 135 K and 2.54(4) Å at 21 K, a shortening that reinforces a second CH···O interaction. By contrast, the corresponding distances Cl6B···O4A and O4B···H5A become much longer than svdWr, 3.637(2) and 2.98(3) Å, respectively. Furthermore, the angle O4B···H5A−C5A becomes much narrower than that at 135 K, 105(2)° vs 117(1)°, while the corresponding angle O4A···H5B−C5B widens to 128(2)°, a value well within the range (115.7−159.6°) of the C−H···O angles found in DMACB for the intercolumn interactions classified as true hydrogen bonds.[39]

4.4. Topological Analysis of the Charge Density. Because of the relatively small number of X-ray measured intensities greater than 2 esd's (Table 1), which is a common threshold limit for data reliability, the experimental charge density distribution ρ_{EXP} at T = 135 K appears of rather modest quality, as judged from the high esd's of the model parameters and derived quantities. Therefore, we consider more appropriate to present the results obtained from the analysis of the theoretical electron density distribution ρ_{THEO}, which shows essential features not significantly different from those of ρ_{EXP}.

The quantities of main interest for the present study are the atomic charges and volumes, together with a detailed description of the anisotropic distribution of the charge density as revealed by its Laplacian, $\nabla^2\rho$. Table 2 reports the results of the QTAIM partitioning of the theoretical electron density of crystalline DCBQ at both T = 135 and 21 K. Charge and volume values, to be discussed in the next paragraph, refer to single molecules extracted from the crystals and are based on a cutoff of ρ = 0.001 atomic units. Details of the procedure adopted by PAMoC to evaluate these quantities have been previously reported.[19b] For the sake of comparison, we list in Table S6 (Supporting Information) the corresponding values for gas-phase DCBQ, as derived by a QTAIM partitioning of ρ calculated with the two different basis sets quoted in the Theoretical Methods section above and the same 0.001 atomic units cutoff.

As previously described, relevant features of the crystal packing associated with the phase transition of DCBQ are, besides the well-known and understood C═O···C═O and C−H···O interactions, the increase in number of very short Cl···Cl separations and the shortening by 0.172 Å of a Cl···O contact. These two latter types of interaction were analyzed by mapping ρ_{THEO} at both T = 135 and 21 K in the corresponding regions and searching for the presence of (3, −1) bond critical points (bcp's). A full description of the aspherical electron density around the Cl and O atoms was then obtained through maps of $\nabla^2\rho$.

Figure 5 shows three plots of $\nabla^2\rho$, pertinent to two interactions at T = 135 K, namely, Cl6···Cl6 (at 2 − x, 1 − y, 1 − z) and Cl6···Cl2 (at 1 + x, 3/2 − y, 1/2 + z), and one at T = 21 K, Cl6A···O4B (at 1 + x, 1 + y, z). In all three cases, a bcp

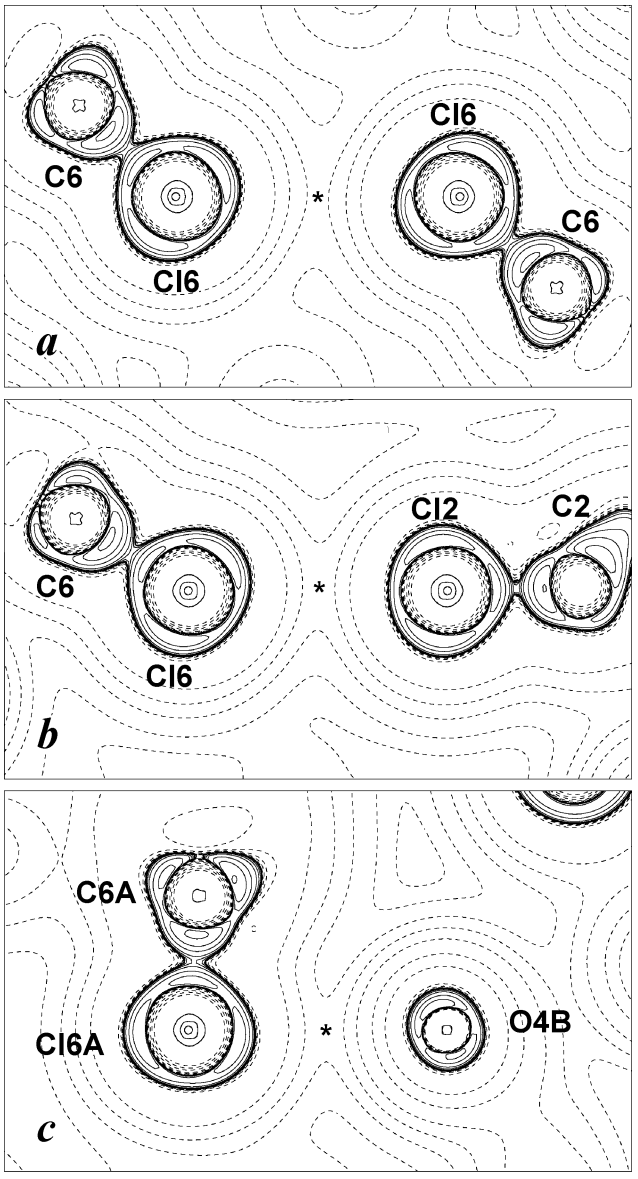

Figure 5. Maps of the negative Laplacian of ρ_{THEO} ($-\nabla^2\rho$) in the region of three short contacts. The contour levels range between ±192.9 e Å^{-5} (corresponding to ±8.0 au), with steps taken at variable intervals. Full lines: positive values, denoting charge concentration. Dotted lines: negative values. (a, b) High-T phase. (c) Low-T phase. In each map, the position of the bcp in the charge density distribution is marked with an asterisk. In (a), the atoms Cl6 and C6 on the right are related to those on the left by the center of inversion at (1, 1/2, 1/2), which coincides with a bond critical point. In (b), the atom C2 lies at 0.185 Å from the plane of the map, defined by the other three atoms.

dx.doi.org/10.1021/cg401123s | Cryst. Growth Des. 2013, 13, 4571−4582

was found analyzing ρ along the bond path connecting each pair of atoms of the short contact.

Full topological and geometrical details of the most relevant interactions in the high-T phase are reported in Table S7 (Supporting Information); those of the low-T phase are in Table S8 (Supporting Information). The absence of bcp's for the short contacts O1···C2 and O1···C6 is not a surprise: the true bonded interaction is between O1 and C1; the other two distances are necessarily short, once the contact O1···C1 has taken place, due to the arrangement adopted by the molecules along the 2_1 axis.

The lack of bcp for the separations C4···O1 at T = 135 K and C4B···O1B at T = 21 K is less justifiable, in view of the close geometrical similarity with the contacts C1···O4 and C4A···O1A, respectively, where the bcp was found, and might indicate an insufficient description of the deformation of ρ by the multipole models. An overall representation of the charge density distribution on the two carbonyl groups and the corresponding intermolecular region at T = 135 K is given in Figure 6, again through a map of $-\nabla^2\rho$ as in Figure 5.

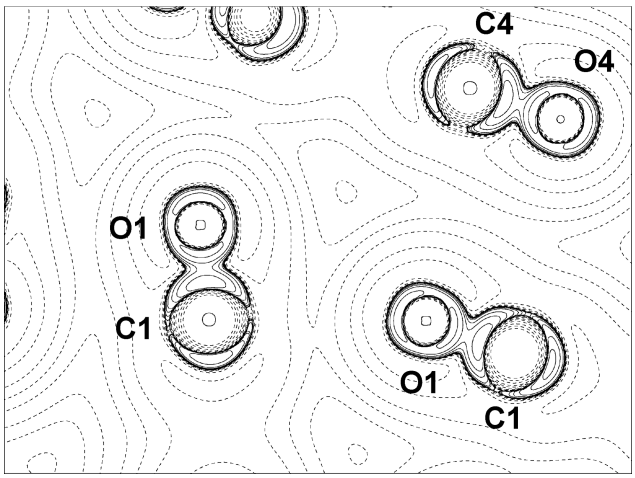

Figure 6. $-\nabla^2\rho$ map in the plane defined by the O1 atoms of two contiguous carbonyl groups and the bond critical point of the intermolecular O1═C1···O1═C1 contact. The two C1 atoms are out of plane by +0.036 Å (that on the left) and +0.100 Å (the one on the right), respectively. Distances from the plane for the atoms of the other carbonyl group C4═O4 are −0.030 Å for the C atom and +0.049 Å for the O atom. Contour levels as in Figure 5.

4.5. Integrated Properties. *4.5.1. Atomic QTAIM Charges.* The atomic charges of the six carbon atoms of crystalline DCBQ remain essentially the same in both phases and in both molecules A and B of the 21 K structure. Indeed, each individual q_C value does not differ by more than 2 esd's with respect to the average of the three determinations, with the exception of atom C4B, where the maximum difference amounts to 3.5 esd's. As for the outermost atoms, all involved in short intermolecular contacts, we observe that, on going from the high-T to the low-T phase, the positive charges of all the H and Cl atoms increase, while the O atoms become more negative. More in detail: at 135 K, atom O1 is more negative than O4 by 0.036 e, and the difference increases, on average, to 0.078 e on going from 135 to 21 K. In terms of estimated standard deviations, the largest variation between the two phases, 10.3 esd's, is observed for atom O1B. We may state that the structural phase transformation of DCBQ is characterized by a well-defined redistribution of the atomic charges at the periphery of the molecule, with a 75% increase of the molecular dipole moment on going from the high-T to the low-T phase (0.36 vs 0.63 D, with a pooled standard deviation of 0.12 D).

There is a striking difference between solid-phase and gas-phase values for the charges of the two C−Cl groups: Cl atoms are negative in the gas phase and significantly positive in the crystals, whereas the opposite occurs to the C atoms bonded to the halogens. Positive values for chlorine atoms are rare: they were found, for example, in 2,5-dichloro-1,4-benzoquinone[40] (as derived from multipolar refinements but not QTAIM integrated), and in 4 out of 21 investigated complexes[41a] formed between halogen-containing molecules and ammonia.

4.5.2. Atomic Volumes. In general, relevant changes of atomic volumes between the gas-phase and the in-crystal $\rho(\mathbf{r})$ fields are useful to investigate how intermolecular contacts trigger a redistribution of the charge density of individual atomic basins.[19a] The balance among the relative strengths of the various classes of intermolecular interactions acting at each specific molecular site determines how the corresponding atomic volume will change on going from the gas phase to the bulk. In both phases of solid DCBQ, all the exocyclic atoms (O, Cl, and H) undergo a significant reduction of their basins upon crystallization, with major changes affecting oxygens (from ≈ −14% to ≈ −24%) and hydrogens ($<\Delta V>$ = −10.2(7)%), whereas chlorines are less influenced ($<\Delta V>$ = −4.1(6)%) by the crystal environment. This clearly mirrors the tendency of exocyclic atoms to set up several interactions, mostly strong and directional, in the bulk. However, while the volume reduction of hydrogen atoms simply reflects their loss of charge due to the formation of CH···O HB contacts,[42] the picture is somewhat more complicated for the O and Cl species.

The volume of O1 is always slightly (0.2−0.6 Å^3) greater than that of O4, mirroring its larger negative charge and implying a lower volume reduction with respect to the isolated molecule. In any case, the important shrinkage of the O1 and O4 basins in both the solid phases (significantly the highest among the exocyclic atoms) signals that, in the crystal, they are involved in particularly strong and close intermolecular contacts.

As for the Cl atoms, we note that our solid-state estimates for their volumes agree well with recent results in crystalline hexachlorobenzene (27.4−28.4 Å^3),[43] while gas-phase QTAIM estimates may range[41] from 28.0 to 36.5 Å^3. Here, both the Cl2 and the Cl6 basins undergo a very high loss of electron population upon crystallization (see above), which results in a positive increase (+0.18 e, more than 140% of the original population) of their atomic charges. Accordingly, their QTAIM volumes are also reduced in the bulk, but these changes (ΔV < 5%) are too small to be understood simply in terms of the reduction of their electron population. Rather, other competing factors are likely at stake in determining the interaction mechanism of Cl atoms in DCBQ. Interestingly, the Cl volumes at 21 K are all slightly larger (on average, by 2.9(3)%) than those at the 135 K, even though the overall differences with respect to the gas-phase volumes remain negative. A positive (or, in this case, a less negative) ΔV implies that, at the corresponding bulk sites, the nondirectional dispersive/repulsive balance cannot be disregarded or, equivalently, that Cl···Cl and Cl···O interactions, when binding, do not play a clearly dominant role in determining the interaction topology of DCBQ.

dx.doi.org/10.1021/cg401123s | *Cryst. Growth Des.* 2013, 13, 4571−4582

Table 3. Interaction Energy Contributions (kJ mol^{-1}) for Some Relevant Molecular Pairs of DCBQ (First Line: High-T Phase Structure. Second and Third Lines: Corresponding Interactions in the Low-T Phase)

mol. pair	symmetry operations[a]	d_{CoM}[b]/Å	shortest contact (sc)	length/Å of sc	E_{es}	E_{rep}	E_{disp}	total $E_{interaction}$
P1	HT1[c]	4.638	C1···O1	2.765	−17.02	11.30	−21.43	−27.15
	A1-B1[d]	*4.613*	*C1A···O1B*	*2.757*	*−18.86*	*12.30*	*−22.15*	*−28.71*
	A1-B2[d]	*4.603*	*O1A···C1B*	*2.734*	*−17.34*	*12.11*	*−22.18*	*−27.41*
P2	HT2[c]	5.426	C4···O1	3.013	−23.55	8.26	−18.90	−34.19
	A1-A2[d]	*5.370*	*C4A···O1A*	*2.992*	*−23.41*	*8.97*	*−19.78*	*−34.22*
	B1-B2[d]	*5.370*	*O1B···C4B*	*2.969*	*−26.18*	*10.44*	*−20.90*	*−36.64*
P3	HT3[c]	5.662	H3···Cl2	3.545	−3.52	5.11	−14.78	−13.19
	A1-A3[d]	*5.721*	*Cl2A···H3A*	*3.340*	*−11.28*	*8.27*	*−17.15*	*−20.16*
	B1-B3[d]	*5.475*	*C2B···H3B*	*3.560*	*−4.58*	*5.26*	*−15.84*	*−15.16*
P4	HT4[c]	6.451	O4···H5	2.71	−14.63	4.25	−9.52	−19.90
	A1-B4[d]	*6.296*	*O4A···H5B*	*2.54*	*−11.21*	*6.45*	*−11.10*	*−15.86*
	A1-B5[d]	*6.608*	*H5A···O4B*	*2.98*	*−17.66*	*3.53*	*−8.67*	*−22.80*
P5	HT5[c]	7.403	H3···O4	2.34	−24.71	18.30	−11.81	−18.22
	A1-A4[d]	*7.488*	*H3A···O4A*	*2.32*	*−37.39*	*16.97*	*−11.07*	*−31.49*
	B1-B6[d]	*7.377*	*H3B···H3B*	*2.32*	*−27.06*	*17.53*	*−11.81*	*−21.34*
P6	HT6[c]	8.258	Cl2···O1	6.565	−2.85	0.00	−0.72	−3.57
	A1-A5[d]	*8.189*	*Cl2A···Cl2A*	*6.249*	*−2.63*	*0.00*	*−0.83*	*−3.46*
	B1-B7[d]	*7.950*	*Cl2B···O1B*	*6.455*	*−4.60*	*0.00*	*−0.82*	*−5.42*
P7	HT7[c]	8.394	Cl2···H5	3.565	1.18	0.49	−2.74	−1.07
	A1-B8[d]	*8.829*	*H3A···H5B*	*3.95*	*0.75*	*0.09*	*−1.59*	*−0.75*
	A1-B9[d]	*8.129*	*H5A···Cl2B*	*3.323*	*3.74*	*1.43*	*−4.12*	*1.05*
P8	HT8[c]	8.784	Cl2···Cl6	3.288	−6.29	5.62	−4.14	−4.81
	A1-B10[d]	*8.632*	*Cl6A···Cl2B*	*3.279*	*−4.75*	*5.81*	*−4.30*	*−3.24*
	A1-B11[d]	*8.912*	*Cl2A···Cl6B*	*3.335*	*−4.02*	*4.79*	*−3.89*	*−3.12*
P9	HT9[c]	8.865	Cl6···Cl6	3.597	−5.61	1.95	−2.95	−6.61
	A1-A6[d]	*8.722*	*Cl6A···Cl6A*	*3.370*	*−9.05*	*4.25*	*−3.85*	*−8.65*
	B1-B8[d]	*9.102*	*Cl6B···Cl6B*	*4.179*	*2.29*	*0.27*	*−1.71*	*0.85*

[a]The first molecule of a pair in the high-T phase is always the molecule at x, y, z, and only the symmetry operation (HTn) to generate the second molecule is given. For the low-T phase, the symmetry operations (An and Bn) are given for both molecules of the pair. [b]Distance between the centers of mass of the two molecules. [c]HT1: $1-x, -1/2+y, 1/2-z$; HT2: $x, -1+y, z$; HT3: $1-x, 1-y, -z$; HT4: $2-x, -1/2+y, 1/2-z$; HT5: $1-x, -y, -z$; HT6: $1-x, 2-y, -z$; HT7: $-1+x, 1/2-y, -1/2+z$; HT8: $-1+x, 3/2-y, -1/2+z$; HT9: $2-x, 1-y, 1-z$. [d]A1: A at x, y, z; A2: A at $x, -1+y, z$; A3: A at $1-x, 1-y, -z$; A4: A at $1-x, -y, -z$; A5: A at $1-x, 2-y, -z$; A6: A at $2-x, 1-y, 1-z$. B1: B at x, y, z; B2: B at $x, 1+y, z$; B3: B at $1-x, -y, 1-z$; B4: B at $1+x, y, z$; B5: B at $1+x, 1+y, z$; B6: B at $1-x, -1-y, 1-z$; B7: B at $1-x, 1-y, 1-z$; B8: B at $-x, -y, -z$; B9: B at $2-x, -y, 1-z$; B10: B at $2-x, 1-y, 1-z$; B11: B at $-x, 1-y, -z$.

4.6. Intermolecular Interaction Energies. Estimates of the total interaction energies $E_{interaction}$ and of the E_{es}, E_{rep}, and E_{disp} terms for nine relevant molecular pairs of DCBQ at 135 and 21 K are reported in Table 3. More details, including all individual components of the electrostatic energy, are given in Table S9 (Supporting Information).

A close inspection of Table 3 shows the following main features: (i) for molecular pairs P1, P2, P3, and P5, the new arrangement of molecules in the low-T phase is more stabilizing than that in the high-T phase; (ii) the same holds, but only on average, for pairs P4 and P6, whereas the opposite is true for pairs P7, P8, and P9; (iii) in all molecular pairs but P3 at 135 K, the E_{es} contribution to the total interaction energy is large and almost always dominant.

From the sum of all the interaction energies of the reference molecule with all the other molecules of the system under study, we have obtained the crystal cohesion energy of DCBQ in the two phases: −258.07 kJ mol^{-1} for the high-T phase and −260.65 kJ mol^{-1} for the low-T phase.

4.7. Crucial Role of Some Atom−Atom Interactions. The dominant crystal packing feature in both high-T and low-T phases is the C═O···C═O separation. On lowering the temperature, hence on reducing the thermal motion, the molecules are more attracted by two types of carbonyl interactions: (i) the C1−O1···C1′ contact, where C1′ is the C1 atom of the contiguous molecule along the screw axis in the monoclinic structure, that reduces from 2.765 Å at T = 135 K to 2.734 and 2.757 Å at 21 K, and (ii) the antiparallel arrangement of two carbonyl groups C1═O1 and C4═O4 of molecules displaced by one periodicity along the b axis, with the two carbonyl groups of molecules A becoming only marginally closer (by ≈0.01 Å), but those of the B molecules reducing their separation by ≈0.05 Å. The electrostatic and attractive nature of both types of C═O···C═O interactions is quantified by the values of the QTAIM charges of Table 2 for their four atoms. Furthermore, Figure 6 illustrates how a region of charge concentration (CC) on atom O1 faces a region of charge depletion (CD) on atom C1, contrary to what happens for the two antiparallel C1═O1 and C4═O4 carbonyl groups, for which a dominant dipole−dipole interaction is easily acknowledged. The "key-lock" scheme of facing CC and CD zones, first presented[44] by Tsirelson, Zou, Tang, and Bader for the shortest intermolecular Cl···Cl separation in solid Cl_2, has been subsequently employed to interpret highly directional interactions between different atomic species (such as, for example, S···N[45,19d] and S···O[19d]) and appears to be, in the words of Scherer and co-workers,[45] "a transferable architectural principle in a molecular crystal". Figure 6 shows that, here in DCBQ, the pattern fits particularly well the C1═O1···C1═O1 interaction.

dx.doi.org/10.1021/cg401123s | Cryst. Growth Des. 2013, 13, 4571−4582

Besides the increased attraction of the carbonyl groups, the decrease of thermal motion favors the enhancement of a Cl···O contact and of a H-bond, as seen above. We remark that the shortening of the two separations Cl6A···O4B (at 1 + x, 1 + y, z) and O4A···H5B (at 1 + x, y, z) is 5 times larger than the shrinkage (0.034 Å) of the a axis due to the reduction of temperature from 135 to 21 K. Furthermore, we note that the type of Cl···O interaction here found (Figure 5c and Table S8, Supporting Information) differs from that recently described[40] for crystalline 2,5-dichloro-1,4-benzoquinone in both geometry and reciprocal arrangement of the anisotropic charge density on the two interacting atoms. Indeed, in DCBQ, the two angles of the sequence C−Cl···O═C are 85.7(1)° and 116.2(2)°, whereas, in the 2,5-dichloro-quinone, the corresponding values are 164.6° and 140.5°. As a consequence, in the latter crystal, a CD region around the chlorine atom faces a CC zone on the oxygen atom, being, therefore, a true halogen bond (XB),[1a,b] whereas, in our case, the opposite occurs and, as seen in Figure 5c, it is the chlorine CC that is closer to the O atom. In both cases, however, oppositely polarized regions are in front of each other; hence the interaction is attractive, electrophilic−nucleophilic in nature.

Whereas, for the Cl···O interaction, the attractive character could have been anticipated by simply considering the QTAIM charges of Table 2, the same does not hold for the halogen−halogen contacts of DCBQ, because all Cl atoms of both high-T and low-T phases are positively charged, as discussed above and shown in Table 2. The Cl···Cl interaction has been deeply investigated,[40,43,46] by both experiment and theory and including extensive searches[46d,g,h] of the Cambridge Structural Database (CSD). Some of the conclusions so far drawn are the following: (i) Cl···Cl interactions are of several types, and it is sometimes difficult to characterize them by using geometrical criteria only.[46e] When such criteria are adopted, the classification of these contacts is based on the value of the two angles, θ_1 and θ_2, of the sequence R--Cl···Cl′--R′; the most common arrangements are those with $\theta_1 = \theta_2$, called type-I (both cis and trans),[46a] and those with $\theta_1 \approx 180°$ and $\theta_2 \approx 90°$, classified as type-II. (ii) The symmetrical type-I contacts are generally considered as van der Waals interactions, whereas the asymmetrical type-II contacts are referred to as polarization induced and understood as attractive $Cl^{\delta+}\cdots Cl^{\delta-}$ interactions. (iii) Interpretations of these interactions in crystal structures based on simple localized charge distributions are unreliable and should be regarded with reserve.[46f] (iv) The most recent works[46a−d] have shown that analyses based either on the molecular electrostatic potential (MEP) or on the electron density distribution are essential to fully characterize these halogen−halogen interactions.

In our case, we have followed both approaches and found that, for crystalline DCBQ, a close examination of the anisotropic features of ρ at the chlorine atoms through Laplacian maps, as in Figure 5a,b, allows a more detailed interpretation than that based on the electrostatic potential $\Phi(\mathbf{r})$ reported in the plot of Figure 7. Nevertheless, the latter, too, clearly indicates the anisotropy of ρ, because the positive electrostatic end cap (σ-hole) on the Cl atoms is a manifestation of "the charge density depletion region localized at the outest region of the halogen"[47] in the direction of the C−Cl bond, a feature that is shown also by a $\Phi(\mathbf{r})$ map of an isolated DCBQ molecule in the gas phase, where the Cl atoms are negatively charged.

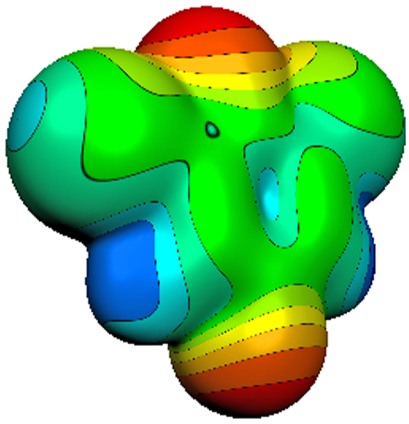

Figure 7. Molecular electrostatic potential mapped on the isodensity surface of 0.01 e Å^{-3} for the DCBQ molecule at 135 K extracted from the crystal. The color scheme ranges from red (negative) via green (neutral) to blue (positive) with values in the range of −153 → +167 kJ mol^{-1}.

It is seen in Figure 5a that even the trans type-I contact Cl6···Cl6, with a distance of 3.597 Å and $\theta_1 = \theta_2 = 136.9°$ at T = 135 K, shows a CC region on one atom facing mainly a CD region on the other, although to a lesser extent than in the optimal arrangements of some X3 synthons of C_6Cl_6[43,46b] or in the case of the L-geometry of 2-chloro-3-chloromethyl-8-methylquinoline.[46a] Hence, at least a partial electrophilic−nucleophilic character can be associated also with this symmetrical type-I interaction. Such a character is maintained at T = 21 K for the contact Cl6A···Cl6A, 3.370 Å long, where the θ angle becomes 143.1° large and the CC-CD pattern is almost unchanged (perhaps is slightly improved; see Figure S1, Supporting Information), whereas, at the much longer (4.179 Å) Cl6B···Cl6B separation, the θ angle narrows to 124.1° and two CC zones face each other almost completely (Figure S2, Supporting Information). It has been reported[46d] that the optimum geometry for trans type-I interactions is $\theta_1 = \theta_2 = 150°$.

As given in Table 3, the Cl6···Cl6 contact is the shortest of the molecular pair P9. Its contribution to the interaction energy of this pair is highly stabilizing in the high-T phase, mainly thanks to an $E_{pro-pro}$ term of −6.13 kJ mol^{-1}, only slightly reduced by $E_{def-def}$ = 0.39 kJ mol^{-1} and somewhat more by E_{rep} = 1.92 kJ mol^{-1}. The prevalence of the electrostatic contribution is increased at 21 K for the contact Cl6A···Cl6A ($E_{pro-pro}$ = −8.34 kJ mol^{-1} vs $E_{def-def}$ = 1.20 kJ mol^{-1} and E_{rep} = 4.21 kJ mol^{-1}), whereas, for the separation Cl6B···Cl6B, an overall destabilizing energy contribution is estimated.

The case of the Cl6···Cl2 interaction illustrated in Figure 5b is one of those that are difficult to classify in terms of geometric criteria, since $\theta_1 = 147.6°$ and $\theta_2 = 173.3°$. Therefore, it seems convenient to interpret it simply as a van der Waals interaction without any further specification. However, here, too, a partial complementarity of CC and CD regions is shown by the Laplacian map and is maintained virtually identical on going to T = 21 K, where a narrowing of 1.9° and 2.5° occurs at θ_1 for the C6A−Cl6A···Cl2B−C2B and C6B−Cl6B···Cl2A−C2A moieties, respectively, together with a larger reduction of 11.1° and 7.4° for the corresponding θ_2 angle. These angular modifications indicate that a compression between the two molecular fragments C6−Cl6 and Cl2−C2 is associated with the phase transition, a process that keeps unchanged at 3.28 Å the halogen−halogen distance in the pair Cl6A···Cl2B but

dx.doi.org/10.1021/cg401123s | Cryst. Growth Des. 2013, 13, 4571−4582

increases it by 0.055 Å in the corresponding pair Cl6B···Cl2A. Despite such a lengthening, this separation and its mate are the shortest of all halogen−halogen distances in the low-T crystal phase of DCBQ, as it was at T = 135 K. It has been stated[46b] that Cl···Cl van der Waals interactions shorter than 3.30 Å are repulsive, but such an assertion was presumably based on the use of the conventional isotropic van der Waals radius, not on the anisotropic model that appears to be necessary for a correct interpretation of −Cl···Cl− intermolecular interactions.[46g] Actually, the energy associated with the high-T phase Cl6···Cl2 contact of Figure 5b, as evaluated by PAMoC,[29] is −4.81 kJ mol^{-1} and becomes −3.24 kJ mol^{-1} for the shorter of the two corresponding contacts at T = 21 K and −3.12 kJ mol^{-1} for the longer contact.

5. CONCLUSIONS

In this work, we have performed a thorough study of the phase transition of crystalline DCBQ and the associated molecular self-recognition process between 21 K and RT. All the relevant NCI interactions and their relative interplay have been characterized by means of geometrical and topological descriptors. The molecular interaction energetics and the crystal cohesive energies of the two phases have also been investigated within the Spackman's model.

We have found that the reduction of thermal motion below T = 130 K favors the enhancement of attractive dipolar carbonyl−carbonyl interactions, which become strong enough to induce a change in the crystal structure, with a progressive, continuous modification of the crystal packing on lowering the temperature to 20 K. The role of a C−H···O hydrogen bond in keeping close to each other two contiguous helices in the high-T phase is maintained almost unchanged in the low-T structure, where another similar H-bond becomes effective in stabilizing the new arrangement of the molecules. The very short halogen−halogen bond that characterizes the monoclinic phase is also maintained as essentially the same in the triclinic structure, but the low-T phase shows a new remarkably short Cl···Cl separation, despite the positive charge on all halogen atoms of solid DCBQ. Besides the relevance of the attractive electrostatic energy of this contact, it is the anisotropic distribution of the charge density around the nuclei of the Cl atoms, as revealed by maps of the Laplacian of ρ, that gives a rationale for their interactions: regions of charge depletion on one atom face regions of charge concentration on the other, with a bond critical point in between, where positive values of both ρ and $\nabla^2\rho$ indicate that the interactions are closed-shell in nature. Dispersive/repulsive nondirectional interactions involving chlorine atoms are also not negligible, and, in fact, they cause the increase of Cl2 and Cl6 integrated volumes on going from 135 to 21 K.

In summary, at least three contributions cooperate in determining the overall nature and strength of the short (<4 Å) Cl···Cl XBs in DCBQ: one of them is repulsive (short-range repulsion), and two of them attractive (electrostatic and dispersive - van der Waals - NCI). Therefore, the Cl···Cl interaction geometries are due to a subtle force balance, which, in turn, determines how molecules in close contact will rotate with respect to each other while T is lowered. Overall, it appears reasonable to state that they act as ancillary to the dominant C═O···C═O interactions, but by no means irrelevant, for the phase transition.

Despite the very low (<1 D) molecular dipole moment of DCBQ, dipolar atom−atom interactions appear as crucial for the observed displacive packing changes through the phase transition. Invariably, their signature in the real-space charge density distribution is the presence of CC zones facing the CD ones of neighboring atomic basins. These features indicate the occurrence of a ubiquitous lock-and-key mechanism for self-recognition in this substance and are also appreciable in the electrostatic potential $\Phi(\mathbf{r})$ maps through the presence of a $\Phi > 0$ end cap (σ-hole) on the halogen atoms.

■ ASSOCIATED CONTENT

Supporting Information

Additional tables with full width at half-maximum (FWHM) for the ω-scan profile of reflection 3 0 −2 as a function of the temperature; cell dimensions in the range of 20−300 K; geometries and intermolecular distances at the three temperatures; results of the rigid-body motion analysis at the three temperatures; QTAIM atomic charges q and volumes V for gas-phase DCBQ; topological and geometrical properties of the most relevant intermolecular interactions of DCBQ at T = 135 and 21 K; figures showing maps of the negative Laplacian of ρ_{THEO} in the region of two Cl···Cl contacts; a table with interaction energy contributions (kJ mol^{-1}) for some relevant molecular pairs of DCBQ, and crystallographic data. This material is available free of charge via the Internet at http://pubs.acs.org. Supplementary crystallographic data for this paper, CIF files, are also deposited at the Cambridge Crystallographic Data Centre with deposition numbers: 941538, 941539, and 941584.

■ AUTHOR INFORMATION

Corresponding Author

*E-mail: riccardo.destro@unimi.it. Fax: +39 02 503 14300. Tel: +39 02 503 14285.

Notes

The authors declare no competing financial interest.

■ REFERENCES

(1) (a) Metrangolo, P.; Resnati, G. *Cryst. Growth Des.* **2012**, *12*, 5835−5838. (b) Desiraju, G. R.; Ho, P. S.; Kloo, L.; Legon, A. C.; Marquardt, R.; Metrangolo, P.; Politzer, P.; Resnati, G.; Rissanen, K. *Pure Appl. Chem.* **2013**, *85*, 1711−1713. (c) Wang, H.; Zhao, X. R.; Jin, W. J. *Phys. Chem. Chem. Phys.* **2013**, *15*, 4320−4328. (d) Legon, A. C. *Angew. Chem., Int. Ed.* **1999**, *38*, 2686−2714.

(2) (a) Hardegger, L. A.; Kuhn, B.; Spinnler, B.; Anselm, L.; Ecabert, R.; Stihle, M.; Gsell, B.; Thoma, R.; Diez, J.; Benz, J.; Plancher, J.-M.; Hartmann, G.; Banner, D. W.; Haap, W.; Diederich, F. *Angew. Chem., Int. Ed.* **2011**, *50*, 314−318. (b) Stone, A. J. *J. Am. Chem. Soc.* **2013**, *135*, 7005−7009.

(3) Martì-Rujas, J.; Colombo, L.; Lü, J.; Dey, A.; Terraneo, G.; Metrangolo, P.; Pilati, T.; Resnati, G. *Chem. Commun.* **2012**, *48*, 8207−8209.

(4) Gavezzotti, A. *Molecular Aggregation: Structural Analysis and Molecular Simulation of Crystals and Liquids*; Oxford University Press: Oxford, U.K.; 2007.

(5) Priimagi, A.; Cavallo, G.; Forni, A.; Gorynsztejn−Leben, M.; Kaivola, M.; Metrangolo, P.; Milani, R.; Shishido, A.; Pilati, T.; Resnati, G.; Terraneo, G. *Adv. Funct. Mater.* **2012**, *22*, 2572−2579.

(6) Viruvuru, V.; Fragata, M. *Phys. Chem. Chem. Phys.* **2008**, *10*, 6607−6614.

(7) Dudekula, S.; Fragata, M. *J. Photochem. Photobiol., B* **2006**, *85*, 177−183.

(8) Fukuzumi, S.; Nakanishi, I.; Suenobu, T.; Kadish, K. M. *J. Am. Chem. Soc.* **1999**, *121*, 3468−3474.

(9) Wenger, O. S.; Leigh, B. S.; Villahermosa, R. M.; Gray, H. B.; Winkler, J. R. *Science* **2005**, *307*, 99−102.

(10) Krongauz, V. V. *J. Phys. Chem.* **1992**, *96*, 2609−2613.
(11) Cameron, D. W.; Evans, R. L.; Feutrill, G. I.; Patrick, V. A.; Skelton, B. W.; White, A. H. *Aust. J. Chem.* **2003**, *56*, 1215−1217.
(12) Bell, S. H.; Cameron, D. W.; Feutrill, G. I.; Skelton, B. W.; White, A. H. *Tetrahedron Lett.* **1985**, *26*, 6519−6522.
(13) Alemán, J.; Richter, B.; Jørgensen, K. A. *Angew. Chem., Int. Ed.* **2007**, *46*, 5515−5519.
(14) Winget, P.; Brédas, J. L. *J. Phys. Chem. C* **2011**, *115*, 10823−10835.
(15) Rees, B. *Acta Crystallogr., Sect. B* **1970**, *26*, 1298−1303.
(16) Sartirana, E. Ph.D. Thesis, Università degli Studi di Milano, Milano, Italy, 2006; chapter 6.
(17) Samson, S.; Goldish, E.; Dick, C. J. *J. Appl. Crystallogr.* **1980**, *13*, 425−432.
(18) Destro, R.; Lo Presti, L.; Soave, R.; Goeta, A. E. In *Modern Charge-Density Analysis*; Gatti, C., Macchi, P., Eds.; Springer: Dordrecht, 2012; Chapter 19, pp 659−696.
(19) (a) Saleh, G.; Soave, R.; Lo Presti, L.; Destro, R. *Chem.—Eur. J.* **2013**, *19*, 3490−3503. (b) Destro, R.; Soave, R.; Barzaghi, M. *J. Phys. Chem. B* **2008**, *112*, 5163−5174. (c) Lo Presti, L.; Destro, R. *J. Chem. Phys.* **2008**, *128*, 044710. (d) Lo Presti, L.; Soave, R.; Destro, R. *J. Phys. Chem. B* **2006**, *110*, 6405−6414. (e) Destro, R.; Soave, R.; Barzaghi, M.; Lo Presti, L. *Chem.—Eur. J.* **2005**, *11*, 4621−4634. (f) Forni, A.; Destro, R. *Chem.—Eur. J.* **2003**, *9*, 5528−5537. (g) Destro, R.; Roversi, P.; Barzaghi, M.; Marsh, R. E. *J. Phys. Chem. A* **2000**, *104*, 1047−1054. (h) Roversi, P.; Barzaghi, M.; Merati, F.; Destro, R. *Can. J. Chem.* **1996**, *74*, 1145−1161. (i) Destro, R.; Merati, F. *Acta Crystallogr., Sect. B* **1995**, *51*, 559−570. (j) Destro, R.; Bianchi, R.; Morosi, G. *J. Phys. Chem.* **1989**, *93*, 4447−4457. (k) Destro, R.; Marsh, R. E.; Bianchi, R. *J. Phys. Chem.* **1988**, *92*, 966−973.
(20) (a) Destro, R. *Chem. Phys. Lett.* **1997**, *275*, 463−468. (b) Destro, R. *Chem. Phys. Lett.* **1997**, *278*, 398.
(21) Stewart, R. F.; Spackman, M. A.; Flensburg, C. *VALRAY User's Manual*, Version 2.1; Carnegie Mellon University Press: Pittsburgh/University of Copenhagen Press: Copenhagen, 2000.
(22) Busing, W. R.; Levy, H. A. *Acta Crystallogr.* **1957**, *10*, 180−182.
(23) Sheldrick, G. M. *SHELXL-97*; University of Göttingen: Göttingen, Germany.
(24) Stewart, R. F. *Acta Crystallogr., Sect. B* **1976**, *32*, 565−574.
(25) (a) Roversi, P.; Destro, R. *Chem. Phys. Lett.* **2004**, *386*, 472−478. (b) Munshi, P.; Madsen, A. Ø.; Spackman, M. A.; Larsen, S.; Destro, R. *Acta Crystallogr., Sect. A* **2008**, *64*, 465−475.
(26) Dovesi, R.; Saunders, V. R.; Roetti, C.; Orlando, R.; Zicovich-Wilson, C. M.; Pascale, F.; Civalleri, B.; Doll, K.; Harrison, N. M.; Bush, I. J.; D'Arco, P.; Llunell, M. *CRYSTAL 2006 Users's Manual*; University of Torino: Torino, Italy, 2007.
(27) (a) Lee, C.; Yang, W.; Parr, R. G. *Phys. Rev. B* **1988**, *37*, 785−789. (b) Becke, A. D. *J. Chem. Phys.* **1993**, *98*, 5648−5652.
(28) (a) Bader, R. F. W. *Atoms in Molecules: A Quantum Theory*; Oxford University Press: Oxford, U.K., 1990. (b) Matta, C. F.; Boyd, R. J. *The Quantum Theory of Atoms in Molecules: From Solid State to DNA and Drug Design*; Wiley-VCH Verlag GmbH & Co. KGaA: Weinheim, 2007.
(29) Barzaghi, M. *PAMoC (Version 2002.0) Online User's Manual*; CNR-ASTM, Institute of Molecular Sciences and Technologies: Milano, Italy, 2002. http://www.istm.cnr.it/pamoc/.
(30) Frisch, M. J.; Trucks, G. W.; Schlegel, H. B.; Scuseria, G. E.; Robb, M. A.; Cheeseman, J. R.; Scalmani, G.; Barone, V. et al. *Gaussian 09*, Revision A.02; Gaussian, Inc.: Wallingford, CT, 2009.
(31) (a) Spackman, M. A. *Chem. Phys. Lett.* **2006**, *418*, 158−162. (b) Spackman, M. A.; Weber, H. P.; Craven, B. M. *J. Am. Chem. Soc.* **1988**, *110*, 775−782. (c) Spackman, M. A. *J. Chem. Phys.* **1986**, *85*, 6587−6601.
(32) (a) Buckingham, A. D. In *Physical Chemistry. An Advanced Treatise*; Henderson, D., Ed.; Academic Press: New York, 1970; pp 349−386. (b) Buckingham, A. D. In *Intermolecular Interactions: From Diatomics to Biopolymers*; Pullmann, B., Ed.; Wiley and Sons: Chichester, NY, 1978; pp 1−67.
(33) Schomaker, V.; Trueblood, K. N. *Acta Crystallogr., Sect. B* **1998**, *54*, 507−514.
(34) Madsen, A. Ø. *Struct. Bonding (Berlin, Ger.)* **2012**, *146*, 21−52.
(35) Chu, S. C.; Jeffrey, G. A.; Sakurai, T. *Acta Crystallogr.* **1962**, *15*, 661−671.
(36) Le Roy, A.; Djeteli, G.; Guerin, R. *J. Mol. Struct.* **1990**, *219*, 131−134.
(37) Baudour, J. L.; Delugeard, Y.; Cailleau, H.; Sanquer, M. *Acta Crystallogr., Sect. B* **1981**, *37*, 1553−1557.
(38) van Weperen, K. J.; Visser, G. J. *Acta Crystallogr., Sect. B* **1972**, *28*, 338−342.
(39) Gatti, C.; May, E.; Destro, R.; Cargnoni, F. *J. Phys. Chem. A* **2002**, *106*, 2707−2720.
(40) Hathwar, V. R.; Gonnade, R. G.; Munshi, P.; Bhadbhade, M. M.; Guru Row, T. N. *Cryst. Growth Des.* **2011**, *11*, 1855−1862.
(41) (a) Zou, J.-W.; Lu, Y.-X.; Yu, Q.-S.; Zhang, H.-X.; Jiang, Y.-J. *Chin. J. Chem.* **2006**, *24*, 1709−1715. (b) Zou, J.-W.; Jiang, Y.-J.; Guo, M.; Hu, G.-X.; Zhang, B.; Liu, H.-C.; Yu, Q.-S. *Chem.—Eur. J.* **2005**, *11*, 740−751.
(42) Koch, U.; Popelier, P. L. A. *J. Phys. Chem.* **1995**, *99*, 9747−9754.
(43) Aubert, E.; Lebègue, S.; Marsman, M.; Bui, T. T. T.; Jelsch, C.; Dahaoui, S.; Espinosa, E.; Ángyán, J. G. *J. Phys. Chem. A* **2011**, *115*, 14484−14494.
(44) Tsirelson, V. G.; Zou, P. F.; Tang, T.-H.; Bader, R. F. W. *Acta Crystallogr., Sect. A* **1995**, *51*, 143−153.
(45) Scherer, W.; Spiegler, M.; Pedersen, B.; Tafipolsky, M.; Hieringer, W.; Reinhard, B.; Downs, A. J.; McGrady, G. S. *Chem. Commun.* **2000**, 635−636.
(46) (a) Hathwar, V. R.; Guru Row, T. N. *J. Phys. Chem. A* **2010**, *114*, 13434−13441. (b) Bui, T. T. T.; Dahaoui, S.; Lecomte, C.; Desiraju, G. R.; Espinosa, E. *Angew. Chem., Int. Ed.* **2009**, *48*, 3838−3841. (c) García, P.; Dahaoui, S.; Katan, C.; Souhassou, M.; Lecomte, C. *Faraday Discuss.* **2007**, *135*, 217−235. (d) Awwadi, F. F.; Willet, R. D.; Peterson, K. A.; Twamley, B. *Chem.—Eur. J.* **2006**, *12*, 8952−8960. (e) Reddy, C. M.; Kirchner, M. T.; Gundakaram, R. C.; Padmanabhan, K. A.; Desiraju, G. R. *Chem.—Eur. J.* **2006**, *12*, 2222−2234. (f) Dunitz, J. D.; Gavezzotti, A. *Helv. Chim. Acta* **2002**, *85*, 3949−3964. (g) Price, S. L.; Stone, A. J.; Lucas, J.; Rowland, R. S.; Thornley, A. E. *J. Am. Chem. Soc.* **1994**, *116*, 4910−4918. (h) Desiraju, G. R.; Parthasarathy, R. *J. Am. Chem. Soc.* **1989**, *111*, 8725−8726.
(47) Duarte, D. J. R.; de las Vallejos, M. M.; Peruchena, N. M. *J. Mol. Model.* **2010**, *16*, 737−748.